Biosensors and Bioelectronics 119 (2018) 134–140

Contents lists available at ScienceDirect

Biosensors and Bioelectronics

journal homepage: www.elsevier.com/locate/bios

Cu-Au nanocrystals functionalized carbon nanotube arrays vertically grown on carbon spheres for highly sensitive detecting cancer biomarker

Duy Thanh Tran[a], Van Hien Hoa[a], Le Huu Tuan[a], Nam Hoon Kim[a,*], Joong Hee Lee[a,b,**]

[a] Advanced Materials Institute for BIN Convergence Technology (BK21 Plus Global), Department of BIN Convergence Technology, Chonbuk National University, Jeonju, Jeonbuk 54896, Republic of Korea

[b] Center for Carbon Composite Materials, Department of Polymer-Nano Science and Technology, Chonbuk National University, Jeonju, Jeonbuk 54896, Republic of Korea

ARTICLE INFO

Keywords:
Cu-Au bimetallic nanocrystals
Vertical carbon nanotube arrays
Carbon spheres
Carcinoembryonic antigen detection
Sensing application

ABSTRACT

A three-dimensional hierarchical nanohybrid based on Cu-Au bimetallic nanocrystals integrated carbon nanotube arrays vertically grown on carbon spheres was successfully developed as an active platform for sensing application. Such nanohybrid can provide abundant active sites and act as an exceptional platform for immobilizing highly dense and well-dispersed carcinoembryonic antibody (anti-CEA) to sensitively detect CEA, an emerging biomarker of various cancer diseases. Due to the unique nanoarchitecture with altered electronic structure of Cu-Au bimetallic catalyst and enhanced interactions between components, such nanohybrid based biosensor demonstrated excellent electrochemical performance towards CEA detection with great sensitivity, wide linear detection range (0.025–25 ng/mL), very low limit of detection (0.5 pg/mL), and good selectivity. The results imply that this sensor has great potential to offer essential information for cancer diagnosis and management with great clinical importance.

1. Introduction

The presence of protein biomarkers in blood serum as early recognition signal of disease has been commonly investigated for diagnosis and therapy. Carcinoembryonic antigen (CEA) is a serum protein that is considered as a key factor associated with various cancers, including colon cancer, lung cancer, breast cancer, and ovarian cancer (Becerra et al., 2016; Jayanthi et al., 2017; Tiernan et al., 2013; Verberne et al., 2016). Meanwhile CEA concentrations in non-smoking person and smoking healthy person have been found to be around 2.5 and 5 ng/mL, respectively (Sajid et al., 2008; Zhu et al., 2013), elevated CEA level has been observed in a cancer patient with growth or recurrence of a tumor (Gao et al., 2017). Therefore, detecting serum CEA level enables for early cancer diagnosis and a subsequent successful treatment. Various methods have been used to detect serum CEA level, including radioimmunoassay (Kato and Torigoe, 1977), fluorescence and optical trapping (Hasanzadeh and Shadjou, 2017; Li et al., 2017a, 2017b; Qin et al., 2017; Qiu et al., 2017), immunocytochemical method (Nakopoulou et al., 1983), field-effect transistor-based (FET-based) nanobiosensor (Bao et al., 2017), plasmonic nanoimmunosensor (Ahn et al., 2017), and love wave biosensor (Li et al., 2017a, 2017b). However, these methods have disadvantages such as radiation dangers, time-consuming, complex procedure, and high cost of instrument. Thus, other alternatives that are easy to use with portability, rapidity, accuracy, and cost effectiveness are needed.

Recently, CEA detection through electrochemical approach has shown great potential (Liu et al., 2015; Su et al., 2017; Yang et al., 2017; Zhou et al., 2014). However, the decreased stability of electrochemical sensor due to low biocompatibility of immobilization platform surface is a critical issue (Skládal, 1997). Weak biological response signals produced by interactions between antibody and antigen also lead to reduced sensitivity (Chikkaveeraiah et al., 2012). Therefore, developing high control and reliable analytical parameters of an electrochemical platform surface that can effectively immobilize antibody proteins and sensitively convert biological response into a measurable electrochemical signal is very important.

Nanomaterials have played critical roles in the fabrication of biosensors with improved analytical performance (Kumar et al., 2015; Maduraiveeran and Jin, 2017). Among these, gold nanoparticles (Au NPs) have shown high promise due to their unique physicochemical properties (Chen et al., 2015; Li et al., 2014; Priyadarshini and Pradhan, 2017). Au NPs are known to have excellent conductivity, leading to

* Corresponding author.
** Corresponding author at: Advanced Materials Institute for BIN Convergence Technology (BK21 Plus Global), Department of BIN Convergence Technology, Chonbuk National University, Jeonju, Jeonbuk 54896, Republic of Korea.
E-mail addresses: nhk@chonbuk.ac.kr (N.H. Kim), jhl@chonbuk.ac.kr (J.H. Lee).

https://doi.org/10.1016/j.bios.2018.08.022
Received 7 June 2018; Received in revised form 23 July 2018; Accepted 10 August 2018
Available online 11 August 2018
0956-5663/

enhanced electron transfer between redox center and electrode surface (Young et al., 2016). Au NPs can also improve electroactive sites of biosensor electrode, thereby exhibiting a very wide linear detection range (Thanh et al., 2016; Wu et al., 2017). In addition, good biocompatibility, high surface free energy, and ability to capture large amounts of proteins due to high affinity of Au with $-NH_2$ and $-SH$ groups existing on molecules' structures offer high stability and sensitivity for immunosensors (Xu and Han, 2004). To further enhance active sites of Au NPs, another metal can be incorporated with Au in a bimetallic nanostructure to finely tune catalytic properties due to the modification of metallic surface properties. In this context, bimetallic nanostructures show remarkably improved optical, catalytic, and electronic properties compared to their monometallic counterparts (Andolina et al., 2013; Kim et al., 2014; Thanh et al., 2017a, 2017b). These bimetallic nanocrystals might be more suitable as biomolecule labeling tags for electrochemical biosensing applications comparing to monometallic Au NPs (Jia et al., 2015; Tao et al., 2011; Zhang et al., 2016). In this regard, bimetallic Cu-Au nanocrystals have recently attracted considerable attention because of their high activity with low cost of Cu (Bracey et al., 2009; Gawande et al., 2016; Vickers et al., 2017). The combination of Au and Cu can decrease the high cost of Au and improve active surface area of Au toward sensing applications. In addition, it has been confirmed that the use of a promising supporting substrate for attaching metal NPs can enhance electroactive surface area of metal catalyst (Kauffman et al., 2010; Lam and Luong, 2014; Tan et al., 2013; Wildgoose et al., 2006), thus amplifying the final sensitivity of sensor. By this means, uniformity and sizes of NPs can be effectively controlled using an exceptional platform of hierarchical porous carbon-based material. Recent reports have shown that vertical growth of aligned CNTs on micro-carbon spheres (CSs) can achieve intrinsic properties of building block with outstanding advantages, including high conductivity, large surface area, high roughness factor, and good mechanical behavior (Li et al., 2016a, 2016b; Piao et al., 2006; Xiang et al., 2007). Therefore, the incorporation of Cu-Au NPs onto a CNTs-CSs hybrid holds great promise as an excellent platform for immobilizing anti-CEA molecules, thereby achieving highly sensitive sensing toward CEA.

In the current work, we developed a novel platform based on Cu-Au/CNTs-CSs hybrid for CEA electrochemical sensing application. CEA detection was based on peak current change of linear sweep voltammetric (LSV) measurement before and after CEA-anti-CEA reaction using potassium ferricyanide ($K_4[Fe(CN)_6]$) as a redox probe. The Cu-Au/CNTs-CSs nanohybrid demonstrated to be an excellent platform for enhancing output signals of CEA sensors at high sensitivity with low limit of detection (LOD).

2. Materials and methods

2.1. Materials

Hydrogen tetrachloroaurate ($HAuCl_4{\cdot}3H_2O$, ≥ 99.9%), copper nitrate ($Cu(NO_3)_2{\cdot}6H_2O$), β-cyclodextrin (97%), uric acid (UA, ≥99%), glucose (≥ 99.5%), ascorbic acid (AA, ≥ 99.5%), sodium dihydrogen phosphate ($NaH_2PO_4{\cdot}H_2O$, ≥ 98%), sodium monohydrogen phosphate (Na_2HPO_4, ≥99%), potassium ferricyanide ($K_4Fe(CN)_6$), urea, dopamine, lyophilized bovine serum albumin (BSA), immunoglobulin G (IgG, 95%), c-reactive protein (CRP), carcinoembryonic antigen (CEA), and anti-CEA were purchased from Sigma Aldrich Chemicals Co. (USA). CEA ACCEL ELISA Kit was purchased from Cosmojin Tech Co. (Korea). Potassium chloride (KCl, > 99.5%) was obtained from Samchun Co. (Korea). Ultra-pure water obtained with an EYELA Still Ace SA-2100E1 filter from Tokyo Rikakikai Co. (Japan) was used throughout all experiments.

2.2. Synthesis of CSs

The procedure to synthesize CSs began with the use of 60 mL DI water containing 8 g of glucose in an 80 mL Teflon lined-autoclave for a hydrothermal process at 190 °C for 7 h. The obtained product was cleaned three times with DI water followed by freeze-drying process to obtain CSs powder.

2.3. Synthesis of CNTs on CSs

Prior to synthesize CNTs on CSs, a solution of copper nanoparticles (Cu NPs) was prepared according to procedure described previously (Thanh et al., 2018). It was then separated into two parts. CSs were deposited with Cu catalyst by adding them into one part of Cu solution under magnetic stirring condition for 3 h. Subsequently, Cu NP deposited CSs were collected by centrifugation and washed with water several times followed by freeze-drying process. These Cu NP/CSs were loaded into a quartz tube of a CVD system for CNT synthesis at 800 °C for 20 min under atmosphere pressure of Ar (500 sccm), H_2 (50 sccm), and C_2H_2 (35 sccm) followed by a rapid cooling process.

2.4. Synthesis of Cu-Au NPs/CNTs-CSs hybrid

Prior to synthesis of Cu-Au NPs/CNTs-CSs hybrid, CNT-CSs powder was deposited with Cu NPs by immersing in another part of Cu NP solution under mild magnetic stirring condition for 3 h. After Cu NP deposited CNTs-CSs sample was annealed under Ar (100 sccm) and H_2 (50 sccm) environment at 400 °C for 1 h, the material was placed in 5 mM $HAuCl_4$ solution for 3 min for a galvanic reaction. The material was then collected by filtering and washed with water several times to remove unreacted agent. Fig. S1 schematically illustrates the synthesis procedure of Cu-Au NPs/CNTs-CSs hybrids.

2.5. Characterization

An electrochemical analyzer CHI 660D workstation (CH Instruments Inc., USA) was used for all electrochemical experiments. In this context, a three-electrode electrochemical system consisting of a modified glassy carbon electrode (GCE, diameter of 3 mm), a Pt plate, and Ag/AgCl as working, counter, and reference electrodes, respectively, was used. To prepare working electrode, 10 μL ink solution of ethanol containing Cu-Au NPs/CNTs-CSs hybrid (2 mg/mL) was drop-casted on the GCE surface followed by drying at ~ 25 °C for 2 h. Then 10 μL of anti-CEA antibody solution (20 μg/mL) was dropped on the surface of Cu-Au NPs/CNTs-CSs/GCE and incubated at ~ 25 °C for 50 min followed by gently washing with 0.1 M phosphate-buffered saline (PBS) (pH = 7.4). After that, 10 μL of BSA solution (2 mg/mL) was added on the modified GCE surface and incubated for 50 min to block extra sites and reduce non-specific adsorption at ~ 25 °C. The sensor was obtained after washing with PBS solution (pH = 7.4). To detect CEA, 6 μL of CEA solution at a specific concentration was dropped onto the surface of sensor followed by incubation for 50 min at ~ 25 °C. The sensor was washed with PBS and then stored at ~ 4 °C prior to electrochemical measurements.

The performance of the sensor toward CEA detection was probed with $K_4[Fe(CN)_6]$ redox agent in 0.1 M PBS solution and monitored by cyclic voltammetry (CV) and different pulse voltammetry (DPV). Effects of interferents such as urea, dopamine (DA), uric acid (UA), glucose, and ascorbic acid (AA) on CEA detection were also explored using DPV technique.

To determine the possibility of using Cu-Au NPs/CNTs-CSs for CEA detection in real sample, different CEA concentrations in human serum spiked PBS solution were applied. In a typical procedure, blood serum was diluted 1000-fold with 0.1 M PBS followed by spiking with three different known CEA concentrations (5, 10, and 15 ng/mL). Recoveries of CEA concentrations were recorded by measuring peak current

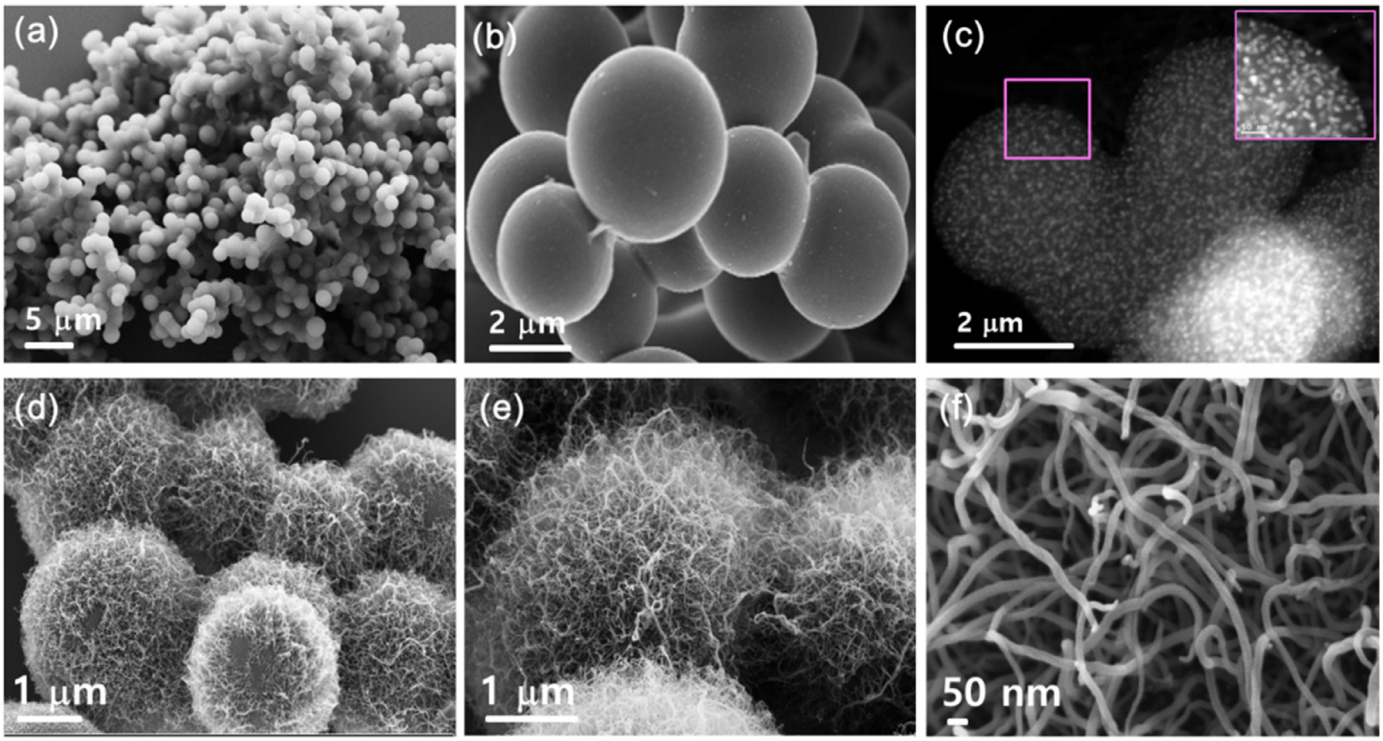

Fig. 1. (a and b) FE-SEM images of as-synthesized CSs; (c) Cu NPs deposited CSs; (d-f) CNTs growth on surface of CSs.

response in DPV.

3. Results and discussion

3.1. Morphological and structural characteristics

Fig. S1 shows the overall procedure for preparing Cu-Au NPs/CNTs-CSs hybrid. First, monodispersed Cu NPs were adsorbed on the surface of as-prepared CSs. CNT bundles were then vertically grown on CSs by CVD method. Finally, Cu-Au NPs were anchored on CNTs surface using a galvanic reaction. Fig. 1 shows representative FE-SEM images of materials at each step for the synthesis of hybrid materials. Fig. 1a and b clearly show uniform and spherical solid CSs with a diameter of 2–3 μm. After Cu NPs were incorporated into CSs, uniform Cu NPs were evenly distributed on the surface of CSs. Corresponding histogram of diameter for Cu NP catalysts indicated that the diameter mainly distributed in the range of 10–15 nm (Fig. S2). As shown in Fig. 1d and e, high density of CNT forest with the length in micrometer range has vertically grown all over CSs, completely covering whole CSs. High magnification FE-SEM image confirmed that the average diameter of CNTs was about 20–30 nm.

The morphology of the Cu-Au NPs/CNTs-CSs nanohybrid was studied by FE-SEM and high-resolution TEM (HR-TEM). Fig. 2a shows FE-SEM image of the CS covered by numerous CNTs functionalized with Cu-Au NPs. High magnification SEM images indicated that uniform size of Cu-Au NPs were homogeneously anchored on CNT surface. This was more pronounced by HR-TEM images, further showing the uniform distribution of metal NPs on the surface of CNTs (Fig. 2d and e). STEM-energy dispersive X-ray (STEM-EDX) line profile elemental mapping for metal NPs showed the presence of Cu (blue line) and Au metal (red line), revealing the formation of a bimetallic nanostructure (Fig. 2f). Such successful achievement of uniform small Cu-Au NPs with high surface to volume ratio and surface energy attached on CNTs-CSs hybrid can provide a more stable surface for immobilizing biomolecules with good retention of their biological activities, thereby capturing more antigens for enhanced sensing performance (Altintas et al., 2014).

XRD characterization was conducted to investigate the crystallinity of as-prepared materials (Fig. 3). It can be seen that there is a broad diffraction peak at 2θ of 21.6° originating from partially amorphous structure of CSs sample (Zhang et al., 2014). The sharper and stronger peak located at higher 2θ of 25.3° for hybrid materials compared to CSs was due to the growth of crystal CNTs on the surface of CSs (Kim et al., 2011). Specific peaks at 43.2, 50.4, and 73.9° corresponded to lattice planes of (111), (200), and (220), respectively, from Cu catalysts in CNTs-CSs after growing CNTs (Rout et al., 2016). In the case of Cu-Au NPs/CNTs-CSs hybrid, in addition to Cu diffraction peaks, specific peak from Au can be observed, suggesting that bimetallic NPs consist of both Au and Cu phases. It is interesting to notice that typical oxide peaks of CuO and Cu_2O phase at 61.7° and 37.5°, respectively, are absent in the hybrid spectra, indicating the formation of an oxide free Cu-Au bimetallic system (Yin et al., 2011).

Raman and XPS analyses were also conducted to investigate the structural characteristics and surface properties of as-prepared materials. The obtained results were shown and detail discussed in Supporting information (Figs. S3 and S4).

3.2. CEA sensing application

The electrochemical sensor toward CEA detection was prepared as shown in Fig. 4a. For electrochemical characterization, CV measurements of CSs, CNTs-CSs, Cu-Au NPs/CNTs-CSs, Anti-CEA/Cu-Au NPs/CNTs-CSs, and BSA/Anti-CEA/Cu-Au NPs/CNTs-CSs modified GCE were investigated in 0.1 M KCl containing 5 mM $K_4[Fe(CN)_6]$ at a scan rate of 50 mV s^{-1} (Fig. 4b). CSs modified GCE gave a pair of redox peaks attributed to redox reaction of $K_4[Fe(CN)_6]$. Compared with CSs/GCE, an increase in peak current intensity was observed on CNTs-CSs/GCE due to the presence of CNTs, which significantly improved electroactive surface area and electrical conductivity. By varing the loading of Cu catalyst deposited on CSs, the influence of grown CNT density on electrochemical behavior of CNTs-CSs/GCE was evaluated. It was found that the CNTs-CSs sample was achieved by depositing CSs with Cu catalyst in 40 mL of the as-prepared solution exhibited better

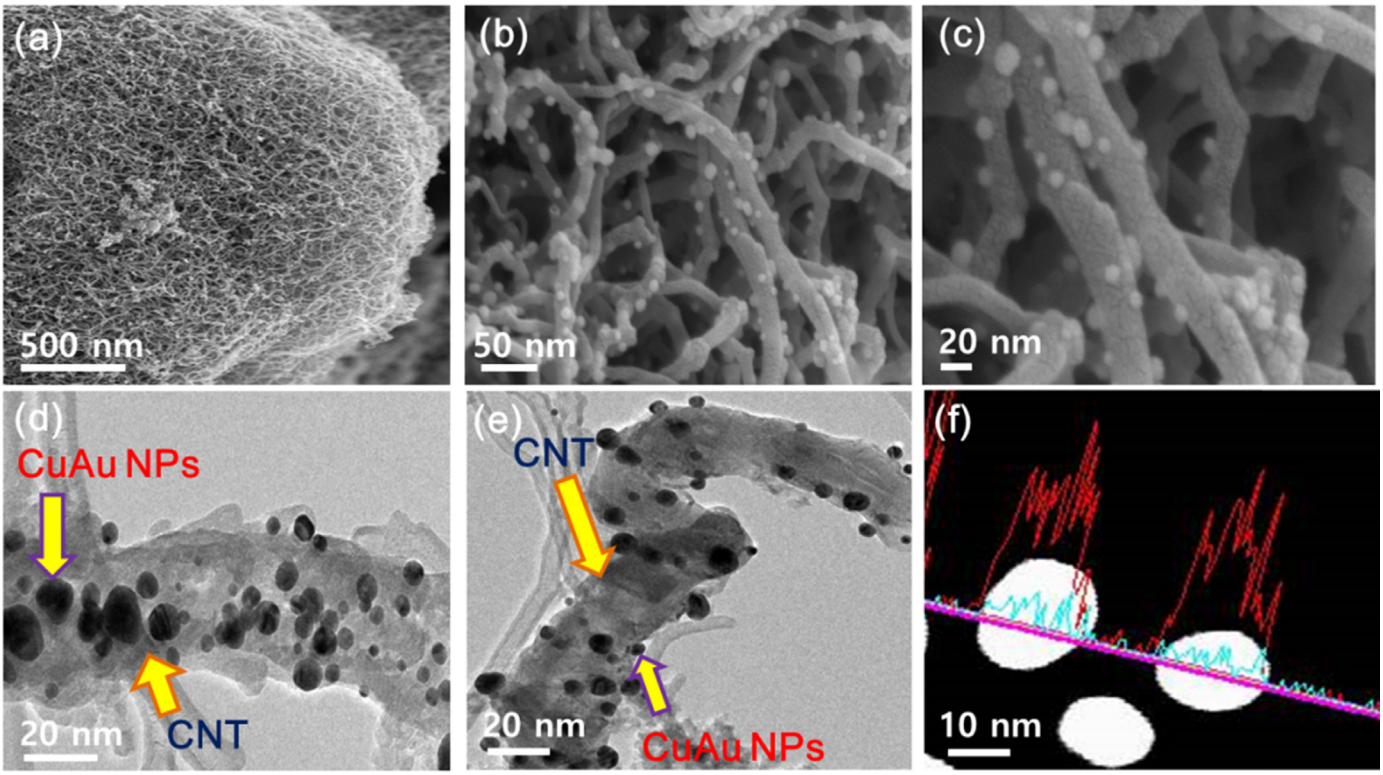

Fig. 2. (a) FE-SEM images of Cu-Au NPs functionalized CNTs-CSs hybrid; (b and c) High magnification FE-SEM images of Cu-Au NPs anchored on CNT surface; (d and e) HR-TEM of Cu-Au NPs functionalized CNT surface; (f) STEM-EDX line profile elemental mapping of Cu-Au NPs on CNT surface.

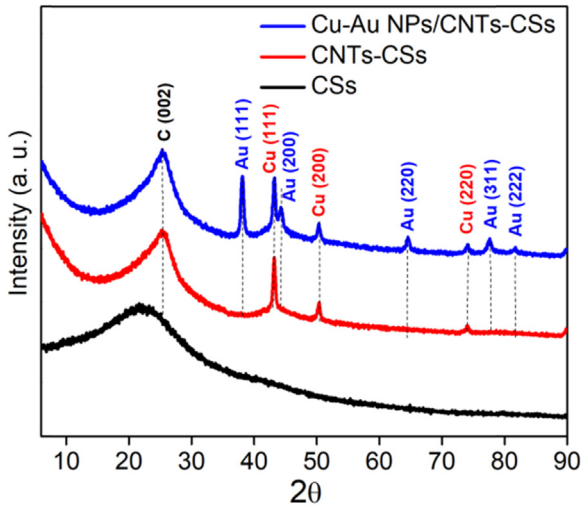

Fig. 3. XRD patterns of CSs, CNTs-CSs, Cu-Au NPs/CNTs-CSs hybrid.

electrochemical response as compared to samples, in which CSs were deposited by catalyst from 40 mL of solutions containing lower and higher Cu content (Fig. S5). The enhanced electrochemical properties were more pronounced when CNTs-CSs hybrid was combined with Cu-Au NPs. An impressive increase in peak current intensity and low peak-to-peak separation (ΔE) indicated that Cu-Au NPs could provide necessary conductive pathways for accelerating electron transfer between the redox probe and the surface of electrode. Therefore, Cu-Au NPs/CNTs-CSs hybrid material can be used as an effective platform for immune sensing application. To optimize suitable amount of Cu-Au NPs/CNTs-CSs for the best electrochemical behavior of electrode, different amounts of Cu-Au NPs/CNTs-CSs ink solution was immobilized on bare GCE surface. As shown in Fig. S6, when 10 μL of Cu-Au NPs/CNTs-CSs ink solution was used, peak current intensity and ΔE values had optimal responses. The use of higher volume of Cu-Au NPs/CNTs-CSs ink solution decreased the electrochemical behavior of electrode because it may lead to growth of film thickness, thereby increasing charge transfer resistance at interfaces (Li et al., 2016a, 2016b). After anti-CEA was deposited on Cu-Au NPs/CNTs-CSs modified GCE, significant reduction of peak current intensity and larger ΔE value can be clearly observed. This indicated that anti-CEA layer was successfully immobilized over on electrode surface, thus effectively hindering electron transfer ability. Additionally, when BSA was applied on electrode surface to block nonspecific binding spots, it also efficiently acted as an electron and mass transfer blocking layer, significantly hindering communication of redox probe with the electrode surface (Güven et al., 2014). In particular, successful capture of CEA on modified electrode surface by forming immunocomplex layer between CEA and anti-CEA was confirmed by critical reduction of peak current (Fig. 4c) (Feng et al., 2013), indicating that the proposed sensor was successfully prepared.

DPV is an effective and sensitive approach to study sensing performance of as-prepared sensor toward CEA. As shown in Fig. 5a, BSA/Anti-CEA/Cu-Au NPs/CNTs-CSs/GCE exhibited a high anodic current response. Compared to BSA/Anti-CEA/Cu-Au NPs/CNTs-CSs/GCE, the current response of CEA/BSA/Anti-CEA/Cu-Au NPs/CNTs-CSs/GCE was dramatically decreased, implying significant prohibition of electrical conductivity due to effective immobilization of CEA on the modified GCE surface. To achieve good performance of the as-prepared sensor, effects of some parameters including incubation time and pH have been investigated. Fig. S7a shows that the best behavior of the sensor can be obtained at pH 7.4. This was due to the fact that proteins can keep their bioactivities at neutral pH environment whereas their activity or linkage can be significantly decomposed in alkaline or acid environment, leading to reduced stability (Li et al., 2015; Tian et al., 2016; Wang et al., 2015). Regarding the effect of incubation time, ΔI value was rapidly increased when incubation time was prolonged from 10 to 50 min. It was then minorly decreased, demonstrating completion

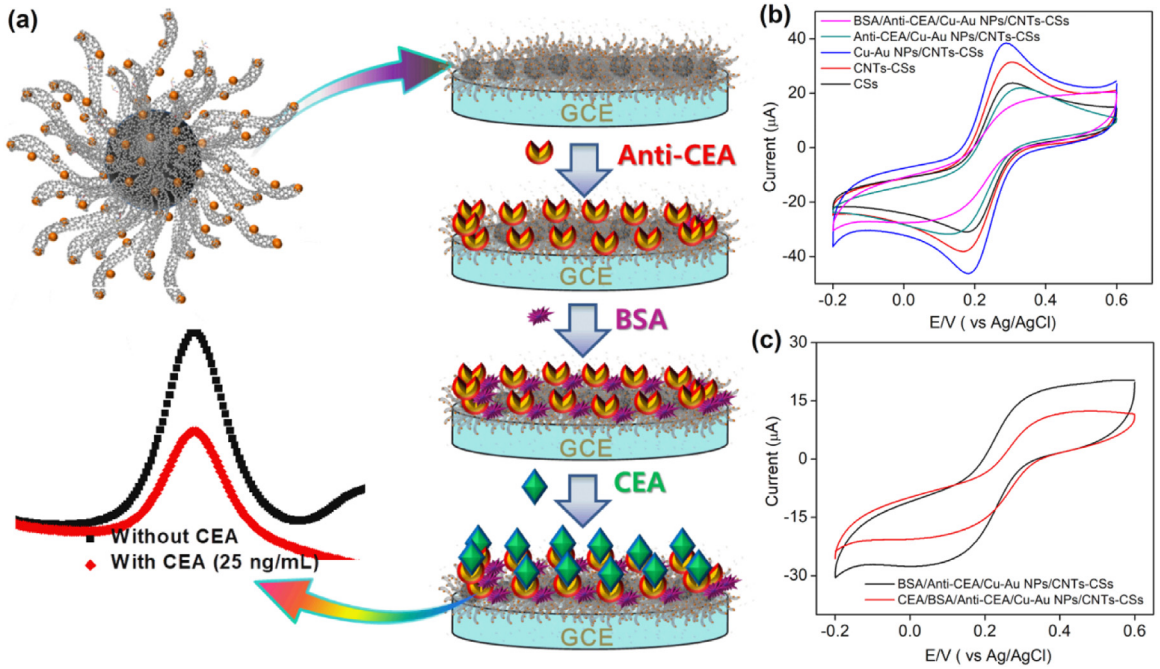

Fig. 4. (a) Schematic illustration of electrochemical sensor fabrication for CEA detection; (b) CV curves of different modified GCE in 0.1 M KCl containing 5 mM $K_4[Fe(CN)_6]$ at a scan rate of 50 mV s^{-1}; (c) CV curves of BSA/Anti-CEA/Cu-Au NPs/CNTs-CSs modified GCE without and with the presence of 25 ng/mL CEA in 0.1 M KCl containing 5 mM $K_4[Fe(CN)_6]$ at a scan rate of 50 mV s^{-1}.

of the reaction between CEA and anti-CEA after 50 min of incubation (Fig. S7b) (Zhu et al., 2013). In another consideration, it was obviously found that there was an increase of ΔI value consistent with the increase of anti-CEA amount and ΔI gradually achieved a plateau state when the anti-CEA content reached to 20 μg/mL (Fig. S8). This implies that the sensor performance depends on the amount of immobilized anti-CEA on the Cu-Au NPs/CNTs-CSs/GCE surface. Therefore, 20 μg/mL of anti-CEA was selected as an optimal content for further reperiments. The specific mechanism for immobilization of anti-CEA on the Cu-Au/CNTs/CSs along with the formation of sensing interface was illustrated in Fig. 5b. In this context, the formation of high Cu-Au NP density attached on CNTs together with the high affinity of Au active sites with $-NH_2$ and $-SH$ groups existing on structure of the anti-CEA molecules allowed a large amount of the anti-CEA molecules to easily immobilize

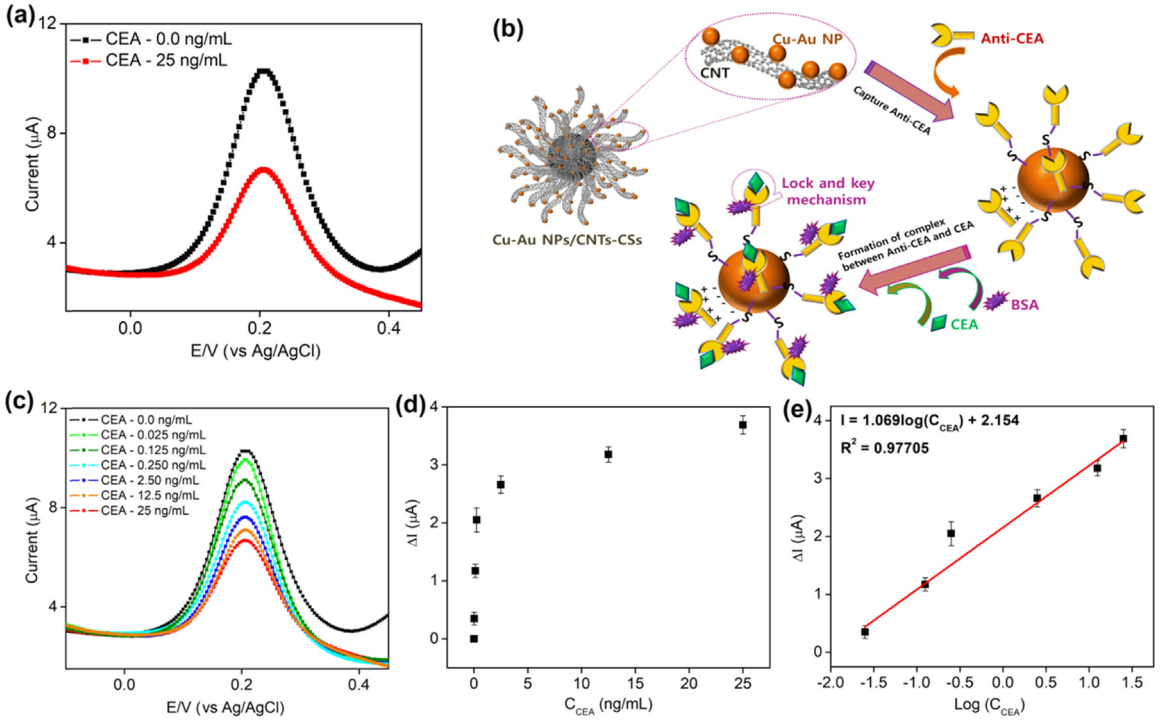

Fig. 5. (a) DPV curves of BSA/Anti-CEA/Cu-Au NPs/CNTs-CSs modified GCE without or with the presence of 25 ng/mL CEA in 0.1 M KCl containing 5 mM $K_4[Fe(CN)_6]$; (b) Schematic illustration for immobilization of anti-CEA and sensing interface on the Cu-Au/CNTs/CSs. (c) DPV curves of BSA/Anti-CEA/Cu-Au NPs/CNTs-CSs modified GCE with the presence of different CEA concentrations; (d) ΔI *vs* C_{CEA}; and (e) The calibration curve of ΔI *vs* log(C_{CEA}).

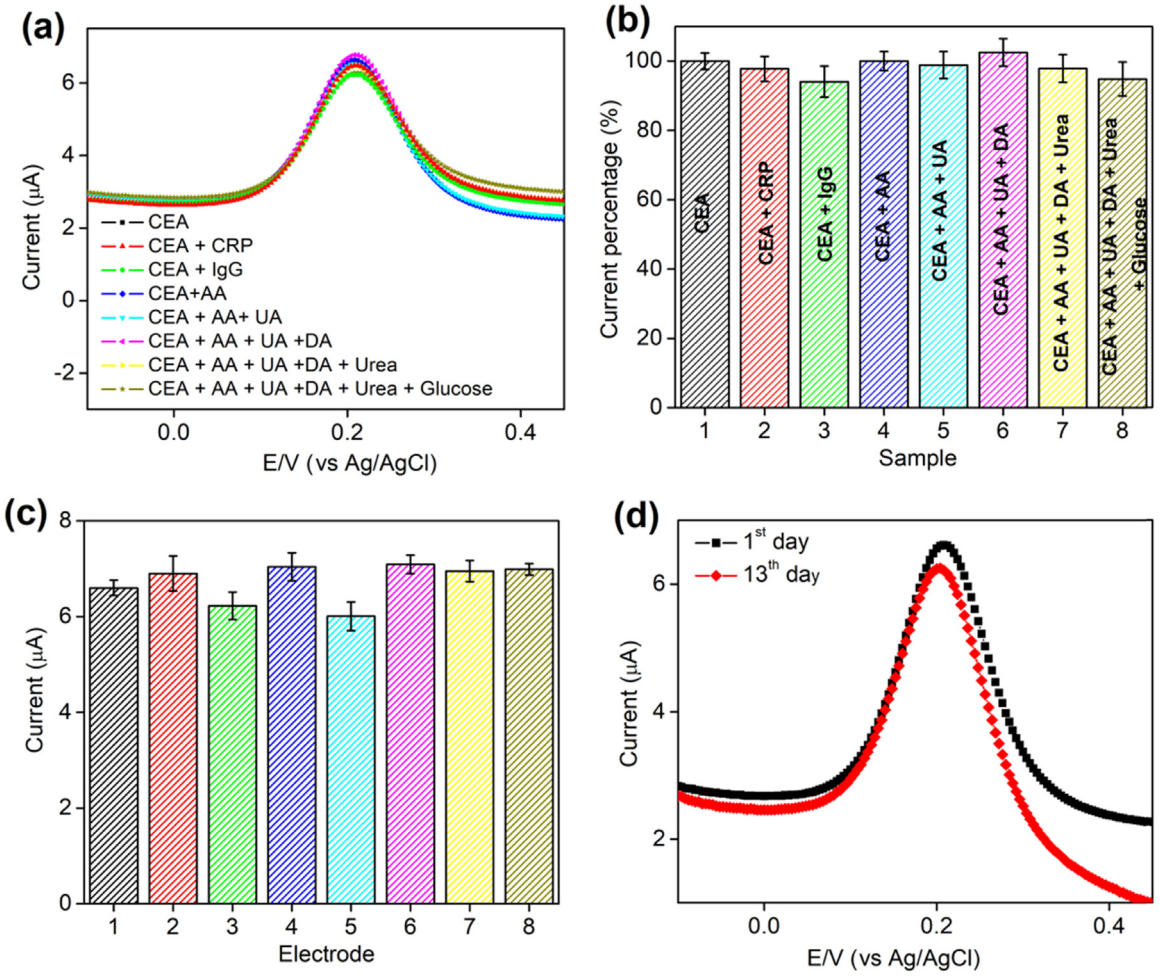

Fig. 6. (a) DPV curves and (b) Change of DPV peak current intensity of BSA/Anti-CEA/Cu-Au NPs/CNTs-CSs modified GCE in the presence of CEA and other biomolecules as interferents in 0.1 M KCl containing 5 mM $K_4[Fe(CN)_6]$; (c) Reproducibility and (d) Stability of as-prepared sensor after long time storage.

onto electrode surface with excellent biocompatibility. This is due to that anti-CEA molecules can adsorb onto the Cu-Au NPs through the covalent bonding, ionic interaction, and hydrophobic interaction (Jazayeri et al., 2016; Xu and Han, 2004). The subsequent incubation of electrode with BSA, a small, stable, low cost, moderately non-reactive protein, can effectively minimize nonspecific binding sites of anti-CEA, thus improving the binding possibility between anti-CEA and CEA (Güven et al., 2014). As a result, the electrode can easily combine with abundant CEA molecules through a lock and key mechanism, thereby reducing background noise and enhancing sensitivity and stability of sensor.

To indicate the enhanced electrochemical sensing performance of Cu-Au/CNTs/CSs material, DPV measurement for Au/CNTs/CSs material was conducted in the presence of 25 ng/mL CEA in 0.1 M KCl containing 5 mM $K_4[Fe(CN)_6]$ at a scan rate of 50 mV s^{-1} for comparison. Fig. S9a indicated the peak current change (ΔI) value of 2.86 μA for Au/CNTs/CSs modified GCE, which is significantly smaller than that of Cu-Au/CNTs/CSs material (ΔI of 3.59 μA) (Fig. S9b). This is because of that the hybridization of Cu and Au could effectively activate the surface of metal NPs in Cu-Au/CNTs/CSs, thereby providing more electroactive sites for efficiently immobilizing anti-CEA molecules.

The sensing performance of such sensor toward different concentration of CEA was evaluated under optimized conditions. DPV results showed that the peak current was gradually decreased with increasing CEA concentration (Fig. 5c). Fig. 5d shows a plot of ΔI against the presence of different CEA concentration. Apparently, ΔI value deflectively increased with increasing CEA value. In this regard, it was found that ΔI value was linearly related to logarithmic values of CEA concentration (log (C_{CEA})) within the range from 0.025 to 25 ng/mL (Fig. 5e). The linear regression equation of the calibration line was found to be $\Delta I = 1.069 \log(C_{CEA}) + 2.154$, with a correlation coefficient (R^2) of 0.97705. A very low LOD was found to be 0.5 pg/mL (S/N = 3). Because normal level of CEA concentration in human serum is around 2–5 ng/mL, the electrochemical behavior of such sensor is completely suitable for clinical analysis toward CEA detection. In order to further demonstrate advantages of such sensor, its performance was compared with previously reported studies (Table S1). In this context, the proposed sensor displayed a comparable practical linear detection range with lower LOD than previously reported studies. These results were attributed to uniform Cu-Au NPs densely attached on a large surface area of a 3D hierarchichal porous CNTs-CSs hybrid which not only provided good electrocatalytic activity and high electron transfer process, but also effectively immobilized with a large amount of biomolecules, thus greatly improving the probability of CEA–anti-CEA recognition with enhanced scope of detection.

Effects of interferences on the activity of sensor toward CEA detection were also evaluated by DPV measurement. In this regard, various common biomolecules presenting in human blood, including c-reactive protein (CRP), immunoglobulin (IgG), and small molecules (such as AA, UA, DA, urea, and glucose) were applied as interferents. BPS solution containing 25 ng/mL CEA, 50 ng/mL of CRP, 50 ng/mL of IgG, and 15 μg/mL of each small molecule interferent was used in this investigation for our proposed sensor. DPV results revealed that current response in the case without and with interferents did not show

significant difference (Fig. 6a). Current percentage varied in the range from 94.1% to 102.5%, implying that such sensor had good selectivity (Fig. 6b). To evaluate the reproducibility of the proposed sensor, different BSA/Anti-CEA/Cu-Au NPs/CNTs-CSs modified electrodes were prepared to detect 25 ng/mL CEA by DPV measurement. The relative standard deviation (RSD) of peak current intensity for eight electrodes was found to be around 6.0%, demonstrating acceptable reproducibility of the sensor (Fig. 6c). In addition to reproducibility of the sensor, the stability of the sensor was also investigated by recording current response in DPV measurements for 25 ng/mL detection after every 2 days. As a result, the current response of sensor remained ~ 94% after 13 days, suggesting that the stability of such sensor was also satisfactory (Fig. 6d).

To evaluate the feasibility of the sensor for real sample detection, recovery test with different CEA concentrations in diluted serum samples was carried out. In this regard, three human serum samples diluted 1000-fold by PBS to avoid nonspecific adsorption phenomenon were prepared in the presence of 5, 10, and 15 ng/mL of CEA (Table S2). Recoveries and RSD of results were found to be in the range of 107.2–108.3% and 5.23–8.19%, respectively. Furthermore, the analytical reliability of the proposed sensor was also confirmed by detecting CEA concentration in three clinical serum samples and was then compared with the obtained results by ELISA kit. Table S3 showed that the RSD% values between two methods were found to be from 7.1% to 8.3%, suggesting good accuracy of the proposed method for detecting CEA in real samples.

4. Conclusion

A novel platform based on Cu-Au NPs/CNTs-CSs hybrid was prepared towards highly sensitive CEA detection for the first time. The fabricated sensor exhibited a wide linear detection range of 0.025–25 ng/mL with low LOD of 0.5 pg/mL, good reproducibility and stability. Besides, the developed sensor showed accurate results for detecting CEA in real samples, implying its possibility in practical application. This was due to the formation of the unique nanostructure in which Cu-Au bimetallic nanocrystals effectively attached on 3D hierarchical CNTs/CSs, thereby offering abundant active sites and excellent platform to immobilize high anti-CEA density for sensitively electrochemical detecting CEA. This sensitive electrochemical sensor shows high potential to detect not just only CEA but also other agents for effective diagnosis and management of many diseases.

Acknowledgements

This research was supported by the Basic Science Research Program (2017R1A2B3004917) through the National Research Foundation (NRF) funded by the Ministry of Science and ICT of Republic of Korea.

Appendix A. Supplementary material

Supplementary data associated with this article can be found in the online version at doi:10.1016/j.bios.2018.08.022.

References

Ahn, S., Yu, H., Kang, S.H., 2017. Biosens. Bioelectron. 96, 159–166.
Altintas, Z., Kallempudi, S.S., Gurbuz, Y., 2014. Talanta 118, 270–276.
Andolina, C.M., Dewar, A.C., Smith, A.M., Marbella, L.E., Hartmann, M.J., Millstone, J.E., 2013. J. Am. Chem. Soc. 135, 5266–5269.
Bao, Z., Sun, J., Zhao, X., Li, Z., Cui, S., Meng, Q., Zhang, Y., Wang, T., Jiang, Y., 2017. Int. J. Nanomed. 12, 4623–4631.
Becerra, A.Z., Probst, C.P., Tejani, M.A., Aquina, C.T., González, M.G., Hensley, B.J., Noyes, K., Monson, J.R., Fleming, F.J., 2016. Ann. Surg. Oncol. 23, 1554–1561.
Bracey, C.L., Ellis, P.R., Hutchings, G.J., 2009. Chem. Soc. Rev. 38, 2231.
Chen, L.Y., Wang, C.W., Yuan, Z., Chang, H.T., 2015. Anal. Chem. 87, 216–229.
Chikkaveeraiah, B.V., Bhirde, A.A., Morgan, N.Y., Eden, H.S., Chen, X., 2012. ACS Nano 6, 6546–6561.
Feng, D., Lu, X., Dong, X., Ling, Y., Zhang, Y., 2013. Microchim. Acta 180, 767–774.
Gao, Y., Song, P.P., Li, H., Jia, H., Zhang, B.J., 2017. BMC Cancer 17, 1–7.
Gawande, M.B., Goswami, A., Felpin, F.X., Asefa, T., Huang, X., Silva, R., Zou, X., Zboril, R., Varma, R.S., 2016. Chem. Rev. 116, 3722–3811.
Güven, E., Duus, K., Lydolph, M.C., Jørgensen, C.S., Laursen, I., Houen, G., 2014. J. Immunol. Methods 403, 26–36.
Hasanzadeh, M., Shadjou, N., 2017. Rev. Microchim. Acta 184, 389–414.
Jayanthi, V.S.P.K.S.A., Das, A.B., Saxena, U., 2017. Biosens. Bioelectron. 91, 15–23.
Jazayeri, M.H., Amani, H., Pourfatollah, A.A., Pazoki-Toroudi, H., Sedighimoghaddam, B., 2016. Sens. Bio-Sens. Res. 9, 17–22.
Jia, H., Gao, P., Ma, H., Wu, D., Du, B., Wei, Q., 2015. Bioelectrochemistry 101, 22–27.
Kato, H., Torigoe, T., 1977. Cancer 40, 1621–1628.
Kauffman, D.R., Sorescu, D.C., Schofield, D.P., Allen, B.L., Jordan, K.D., Star, A., 2010. Nano Lett. 10, 958–963.
Kim, D., Resasco, J., Yu, Y., Asiri, A.M., Yang, P., 2014. Nat. Commun. 5, 1–8.
Kim, J.Y., Park, K., Bae, S.Y., Kim, G.C., Lee, S., Choi, H.C., 2011. J. Mater. Chem. 21, 5999.
Kumar, S., Ahlawat, W., Kumar, R., Dilbaghi, N., 2015. Biosens. Bioelectron. 70, 498–503.
Lam, E., Luong, J.H.T., 2014. ACS Catal. 4, 3393–3410.
Li, C.Y., Cao, D., Qi, C.B., Chen, H.L., Wan, Y.T., Lin, Y., Zhang, Z.L., Pang, D.W., Tang, H.W., 2017a. Biosens. Bioelectron. 90, 146–152.
Li, F., Jiang, L., Han, J., Liu, Q., Dong, Y., Li, Y., Wei, Q., 2015. RSC Adv. 5, 19961–19969.
Li, F., Li, Y., Dong, Y., Jiang, L., Wang, P., Liu, Q., Liu, H., Wei, Q., 2016a. Sci. Rep. 6, 1–10.
Li, N., Zhao, P., Astruc, D., 2014. Angew. Chem. - Int. Ed. 53, 1756–1789.
Li, S., Wan, Y., Su, Y., Fan, C., Bhethanabotla, V.R., 2017b. Biosens. Bioelectron. 95, 48–54.
Li, Y., Li, D., Rao, Y., Zhao, X., Wu, M., 2016b. Carbon 105, 454–462.
Liu, J., Wang, J., Wang, T., Li, D., Xi, F., Wang, J., Wang, E., 2015. Biosens. Bioelectron. 65, 281–286.
Maduraiveeran, G., Jin, W., 2017. Trends Environ. Anal. Chem. 13, 10–23.
Nakopoulou, L., Zinozi, M., Theodoropoulos, G., Papacharalampous, N., 1983. Dis. Colon Rectum 26, 269–274.
Piao, Y., An, K., Kim, J., Yu, T., Hyeon, T., 2006. J. Mater. Chem. 16, 2984.
Priyadarshini, E., Pradhan, N., 2017. Sens. Actuators B Chem. 238, 888–902.
Qin, W., Wang, K., Xiao, K., Hou, Y., Lu, W., Xu, H., Wo, Y., Feng, S., Cui, D., 2017. Biosens. Bioelectron. 90, 508–515.
Qiu, Z., Shu, J., Tang, D., 2017. Anal. Chem. 89, 5152–5160.
Rout, L., Kumar, A., Dhaka, R.S., Dash, P., 2016. RSC Adv. 6, 49923–49940.
Sajid, K.M., Chaouachi, K., Mahmood, R., 2008. Harm Reduct. J. 5, 1–14.
Skládal, P., 1997. Electroanalysis 9, 737–745.
Su, S., Han, X., Lu, Z., Liu, W., Zhu, D., Chao, J., Fan, C., Wang, L., Song, S., Weng, L., Wang, L., 2017. ACS Appl. Mater. Interfaces 9, 12773–12781.
Tan, C., Huang, X., Zhang, H., 2013. Mater. Today 16, 29–36.
Tao, M., Li, X., Wu, Z., Wang, M., Hua, M., Yang, Y., 2011. Clin. Chim. Acta 412, 550–555.
Thanh, T.D., Balamurugan, J., Hien, H., Van, Kim, N.H., Lee, J.H., 2017a. Biosens. Bioelectron. 96, 186–193.
Thanh, T.D., Balamurugan, J., Hwang, J.Y., Kim, N.H., Lee, J.H., 2016. Carbon 98, 90–98.
Thanh, T.D., Balamurugan, J., Tuan, N.T., Jeong, H., Lee, S.H., Kim, N.H., Lee, J.H., 2017b. Biosens. Bioelectron. 89.
Thanh, T.D., Chuong, N.D., Hien, H.V., Kim, N.H., Lee, J.H., 2018. ACS Appl. Mater. Interfaces 10.
Tian, L., Liu, L., Li, Y., Wei, Q., Cao, W., 2016. Sci. Rep. 6, 1–8.
Tiernan, J.P., Perry, S.L., Verghese, E.T., West, N.P., Yeluri, S., Jayne, D.G., Hughes, T.A., 2013. Br. J. Cancer 108, 662–667.
Verberne, C.J., Wiggers, T., Grossmann, I., de Bock, G.H., Vermeulen, K.M., 2016. Color. Dis. 18, O91–O96.
Vickers, J.W., Alfonso, D., Kauffman, D.R., 2017. Energy Technol. 5, 775–795.
Wang, Y., Ma, H., Wang, X., Pang, X., Wu, D., Du, B., Wei, Q., 2015. Biosens. Bioelectron. 74, 59–65.
Wildgoose, G.G., Banks, C.E., Compton, R.G., 2006. Small 2, 182–193.
Wu, W., Fang, Y., Zhu, C., Chen, S., Li, T., Wu, L., Bao, N., Liu, Y., Gu, H., 2017. RSC Adv. 7, 42884–42890.
Xiang, R., Luo, G., Qian, W., Wang, Y., Wei, F., Li, Q., 2007. Chem. Vap. Depos. 13, 533–536.
Xu, S., Han, X., 2004. Biosens. Bioelectron. 19, 1117–1120.
Yang, Y., Liu, Q., Liu, Y., Cui, J., Liu, H., Wang, P., Li, Y., Chen, L., Zhao, Z., Dong, Y., 2017. Biosens. Bioelectron. 90, 31–38.
Yin, A., Wen, C., Dai, W.-L., Fan, K., 2011. J. Mater. Chem. 21, 8997.
Young, S.L., Kellon, J.E., Hutchison, J.E., 2016. J. Am. Chem. Soc. 138, 13975–13984.
Zhang, H., Ma, L., Li, P., Zheng, J., 2016. Biosens. Bioelectron. 85, 343–350.
Zhang, X., Ma, J., Yang, W., Gao, Z., Wang, J., Liu, Q., Liu, J., Jing, X., 2014. CrystEngComm 16, 4016–4022.
Zhou, J., Du, L., Zou, L., Zou, Y., Hu, N., Wang, P., 2014. Sens. Actuators B Chem. 197, 220–227.
Zhu, L., Xu, L., Jia, N., Huang, B., Tan, L., Yang, S., Yao, S., 2013. Talanta 116, 809–815.